High Efficiency and High Rate Deposited Amorphous Silicon-Based Solar Cells

PHASE III Third Quarter
Technical Progress Report

March 1, 2004 to May 31, 2004

NREL Subcontract No. NDJ-2-30630-08

Subcontractor: The University of Toledo

Principal Investigator: Xunming Deng
                              Department of Physics and Astronomy
                              University of Toledo, Toledo, OH 43606
                              (419) 530-4782
                              dengx@physics.utoledo.edu

Contract technical monitor: Dr. Bolko von Roedern

Modeling of Triple Junction a-Si Solar Cells Using ASA: Analysis of Device Performance Under Various Failure Scenarios

Contributors: Chandan Das and Xunming Deng

Abstract

Triple junction a-Si solar cells have been modeled and simulated using the Advanced Semiconductor Analysis (ASA). The device performance is analyzed with numerically simulated I-V characteristics. We have studied several failure scenarios such as variations in the thickness of different layers of the multilayered triple-junction structure. Distinctive features of the I-V characteristics and solar parameters have been found which have been correlated and discussed with the basis of device physics.

Introduction

Manufacturing activities of amorphous silicon (a-Si) based thin film solar cells have experience a significant increase in the recent years. Solar panels with triple-junction spectrum-splitting structure are being manufactured in high-volume production. In the fabrication of an a-Si/a-SiGe/a-SiGe nip/nip/nip triple cell, the thickness, bandgap and other properties of each of the nine semiconductor layers as well as the other non-semiconductor layers need to be accurately controlled in order for a triple cell to produce its highest power output. An unintentional change, or a "failure", of any one of these layers could lead to undesirable changes in the solar cell I-V characteristics and quantum efficiency. These changes are often abnormal and difficult to understand.

Modeling of triple junction solar cells and numerical simulation of variation in layers to reproduce the effect of variations in the deposition sequence, could help to predict the changes in behavior of the solar cell performance. These predicted results would be extremely helpful to readily point out the failure mechanism by eliminating a large number of possibilities, should any of these failures occur in solar cell fabrication including PV manufacturing. Unfortunately, no reports of comprehensive study of failure analysis for the fabrication of multiple-junction solar cells and/or the comparison of these predicted results with real multi-junction devices have been found. To assist the optimization of solar cell fabrication and cost-effective industrial photovoltaic production, there is a strong need for the study of various possible failure scenarios in the deposition steps associated with the fabrication of multilayered thin film solar cells. In the present work, we selected a number of failure mechanisms that may occur during triple-cell device fabrication and studied the numerically simulated current-voltage (I-V) characteristics using Advanced Semiconductor Analysis (ASA), a program developed by Technical University of Delft.[1] Deviated solar cell I-V characteristics predicted under various failure scenarios are compared to that of a normal case. In the future, we will report cross examination and verification of these predicted I-V performance with that of real triple-junction solar cell devices intentionally fabricated under these failure scenarios.

Modeling

A triple junction a-Si solar cell has been constructed in computer modeling with ASA. The cell has the following structure: Al/n-bottom/i-buffer/i-bottom/i-buffer/p-bottom/n-middle/i-buffer/i-middle/i-buffer/p-middle/n-top/i-top/p-top/TCO and the schematic diagram of this cell is given in Figure 1. This structure is taken as the standard for the present study and its simulated I-V characteristic is designated as the normal case. The other different cases chosen for the present study are shown in the Table 1. When any one layer is varied, all other layers have been kept unchanged in each of these scenarios.
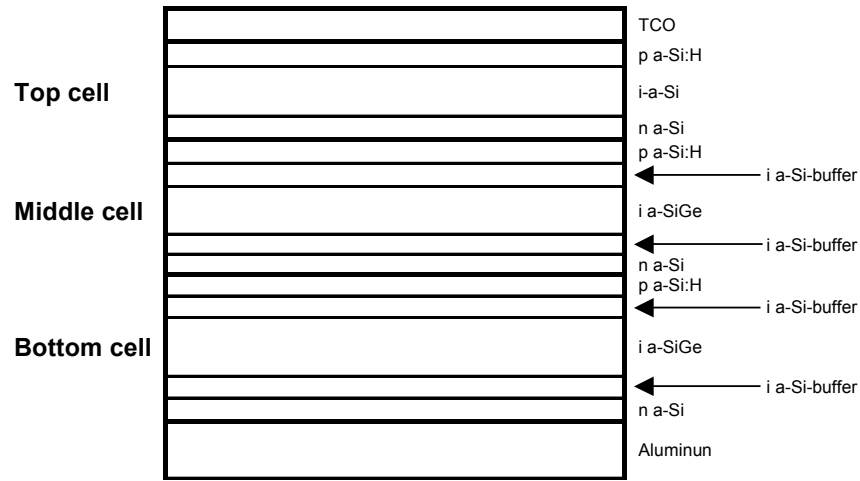

Fig 1: Schematic diagram of the modeled triple junction solar cell.

Table 1: Description of different simulation cases for the triple junction solar cells studied in the present work.

		Cases (In the parenthesis, corresponding figure sub-numbers are given)	
n-layer	Top cell	No layer [A1]	Five times more thickness [A2]
	Middle cell	No layer [B1]	Five times more thickness [B2]
	Bottom cell	-	-
p-layer	Top cell	-	-
	Middle cell	No layer [C1]	Five times more thickness [C2]
	Bottom cell	No layer [D1]	Five times more thickness [D2]
i-layer	Top cell	10nm / 1nm layer [E1]	Five times more thickness [E2]
	Middle cell	-	-
	Bottom cell	10nm layer/ no buffer layers [F1]	Five times more thickness [F2]

Results and discussion

In Figure 2, the dark and illuminated I-V characteristics of all these cases obtained from ASA simulation are shown; the figure sub-numbers correspond to the designated cases in the parenthesis in Table 1. The dark and illuminated I-V characteristics are presented by dotted and solid curves. In the "normal case" studied here, the device shows a I-V characteristics of V_{oc}=2.1V, J_{sc}=7.2 mA/cm^2 and FF=0.60 and the triple-cell current is limited by that of the middle cell under AM1.5 spectrum at the maximum power point. In Case A1, when we skip the n-layer of top cell, V_{oc} drops to 1.4V and short circuit current (J_{sc}) remains almost the same with a slight increase. The lack of the top-cell n-layer leaves the triple junction structure as Al/n-bottom/i-buffer/i-bottom/i-buffer/p-bottom/n-middle/i-buffer/i-middle/i-buffer/p-middle/—/i-top/p-top/TCO, which has low V_{oc} due to the lack of one functioning n-i-p diode. On the other hand, thicker n-layer (Case A2) reduces the J_{sc} to 4.78 mA/cm^2 due to the reduced number of photons absorbed by the current-limiting middle cell, while the V_{oc} stays unchanged.

In Case B1 where middle cell n-layer is skipped, the V_{oc} drops to 1.42V and the FF drops to 0.49 while the J_{sc} remains unchanged. In addition, the I-V characteristic becomes S-shaped with suppressed increase in J_{sc} under forward bias. Further, the dark I-V characteristics shows no switching on of diode operation under forward bias. However, for the thicker middle cell n-layer (B2), no prominent variation is noticed except the reduction of FF to 0.58. We choose not to discuss the modeled results of the effect of the bottom cell n-layer in this report, since the effect of the variation of this layer's thickness depends sensitively on the choice of layer underneath, which is aluminum metal layer in the present study. For a similar reason, the effect of top-cell p-layer is also not discussed in this report.

When the middle-cell p-layer is skipped (C1), V_{oc} is reduced as expected. However, in the case of thicker middle-cell p-layer (C2), we observe a peculiar I-V characteristics along with variation in J_{sc}, V_{oc}, and FF. It appears that under near open-circuit conditions, it is difficult for photo-generated holes to move from the middle-cell i/p interface to the (middle-p)/(top-n) tunnel junction, causing reduced triple-cell current (the kink in the light IV near 1.8V). Similar results are obtained in Cases D1 and D2 where bottom cell p-layer is skipped and made thicker, respectively. The only difference is that the behavior of dark I-V characteristic is different in D1 from that in C1.

In Case E1, where the thickness of the top-cell i-layer is decreased to 1 nm from its 40nm standard case, unexpected results in I-V characteristics has been obtained. In short-circuit condition, the current is diminished while with increase in forward bias (i.e. under loaded condition) current shows an increase. To understand this strange behavior, a case with the thickness of the top-cell i-layer being 10nm was simulated and the peculiar I-V characteristics is also observed, but with less pronounced features. This peculiar IV performances, observed only for much reduced thicknesses than the normal conditions, is not well understood and requires further study. With a top cell i-layer five times thicker (E2) than that of standard, a decrease in J_{sc} is obtained due to the reduced light absorbed by the middle cell which is limiting the current. The V_{oc} and the shape of the I-V

characteristic remain unchanged. In Case E2, there is also an artificial increase in FF due to the increased current mis-match.

In the Cases F1 & F2, we varied the bottom cell i-layer thickness. The J_{sc} is significantly reduced when the bottom cell i-layer is made only 10nm in thickness with both of the buffer layers skipped (Case F1). For Case F2, the thicker bottom-cell i-layer results in almost no change in triple-cell IV, since the J_{sc} is still limited by the middle cell.
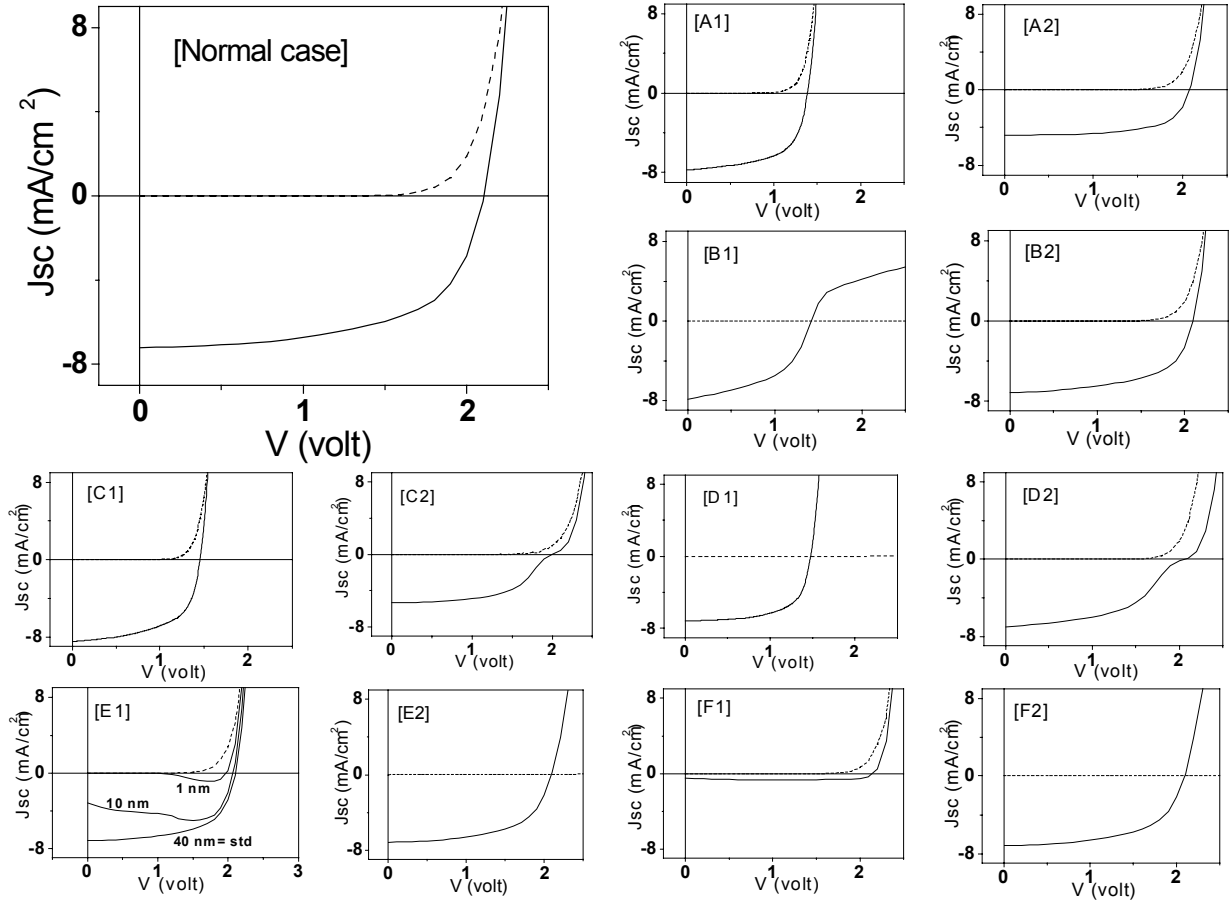

Fig. 2: ASA generated I-V characteristics of the standard triple junction solar cell (Normal case) and cases designated in Table 1 as A1, A2, B1, B2, C1, C2, D1, D2, E1, E2, F1, and F2.

Conclusion

Using ASA generated I-V results of a normal triple-junction a-Si/a-SiGe/a-SiGe solar cell and those under various "failure" conditions, we analyzed the expected and unexpected IV characteristics when one of the doped or undoped layers is made thicker (five times thicker) or thinner (zero thickness or significantly reduced thickness). Various IV performances are predicted under this failure scenarios. These findings and analyses can be used to assist fabrication of triple-

junction a-Si bases solar cells in both research and manufacturing to quickly identified possible failure scenarios, should any of these occur.

References

[1] R. Schropp and M. Zeman, Amorphous and Microcrystalline Silicon Solar Cells, Modeling, Materials and Device Technology, Kluwer Academic Publishers,1998. Part II.

Hydrogenated Nanocrystalline Silicon *p*-Layer in *a*-Si:H *n-i-p* Solar Cells

Contributors:
Univ. of Toledo: W. Du, X. Liao, X.Yang, H. Povolny, X. Xiang, and X. Deng
Univ. of Michigan: K. Sun

Overview

In the last Quarterly report (12/1/03-2/28/04), we discussed the dependence of a-Si nip solar cell Voc on the structure of the p-layer, covering the transition from amorphous → protocrystalline → nanocrystalline+amorphous (nc+a) mixed phase. It is concluded that higher Voc is obtained when the p-layer is made with fine-grained nc-Si mixed with a-Si phase. In this Quarterly report, we discuss the dependence of a-Si nip solar cell Voc on the structure of the p-layer, covering the transition from (nc+a) mixed phase → microcrystalline silicon. It is concluded that Voc drops significantly when the microcrystalline silicon p-layer is used.

Abstract

This paper investigates the impacts of hydrogenated nanocrystalline silicon (*nc*-Si:H) *p*-layer on the photovoltaic parameters, especially the open circuit voltage (V_{oc}) of *n-i-p* type hydrogenated amorphous silicon (*a*-Si:H) solar cells. Raman scattering spectroscopy and transmission electron microscopy (TEM) analyses indicate that this p-layer is a diphasic material that contains nanocrystalline grains with size around 3-5 nm embedded in an amorphous silicon matrix. Optical transmission measurements show that the *nc*-Si *p*-layer has a wide bandgap of 1.96 eV, due to the quantum confinement effects (QCE). Using this kind of *p*-layer in *n-i-p a*-Si:H solar cells, the cell performances were improved with a V_{oc} of 1.042 V, while the solar cell deposited under a similar condition but incorporating a hydrogenated microcrystalline silicon (*μc*-Si:H) *p*-layer leads to a V_{oc} of 0.526 V.

Introduction

The limiting factors of open circuit voltage of *a*-Si:H solar cells have been an interesting topic since *a*-Si:H alloys became a viable material for photovoltaic devices. Theoretical considerations expected that recombination originating from band tail states puts a fundamental limit on the output voltage of *p-i-n a*-Si:H solar cells, and the maximum V_{oc} calculated from the difference between the electron and hole quasi-Fermi levels in the intrinsic (*i*) layer is 1.0 ± 0.1 V.[1] Experimentally, using high hydrogen dilution or hydrogen-plasma treatment, *a*-Si:H solar cells with V_{oc} greater than 1.0 V could be fabricated,[2,3] which is well consistent with the above theoretical estimation.

However, it is noted that this estimate holds only for the situation when the built-in-potential in the *i* layer, set up by the doped (*p* and *n*) layers, is greater than the difference between the electron and hole quasi-Fermi levels. In fact, the doping layers, especially the *p*-layer acting as a window layer in both superstrate and substrate structures, have great influences on V_{oc} available in practical devices.

It was reported that using a *μc*-Si:H *p*-layer in *a*-Si:H *n-i-p* cells with a substrate structure on stainless steel (SS), the cell performance could be improved through an increase in the built-in potential of the junction and a decrease in the series resistance.[4] However, using a *μc*-Si:H *p*-layer in *a*-Si:H *p-i-n* cell with a superstrate structure on SnO$_2$ coated glass, it could induce a disastrous effect on the open circuit voltage and the fill factor (*FF*).[5] In a recent report, R. J. Koval *et al* argued that 10-20 nm thick *p*-layers prepared on *i*-layers under certain conditions may be amorphous even at hydrogen dilution values as high as 200, due to a possible barrier for microcrystal nucleation on an amorphous *i*-layer surface.[6] Moreover, they proposed that the maximum V_{oc} is obtained by incorporating *p*-type doped Si:H layers that are protocrystalline in nature, and even relatively low substrate-induced microcrystalline fractions in the *p*-layer are detrimental.[6]

The question is why the use of a microcrystalline *p*-layer is detrimental for *a*-Si:H cell performances? An explanation was that this is due to the narrow bandgap (E_g) of *μc*-Si:H *p*-layer and a barrier at the *p/i* interface caused by the band offset between microcrystalline *p*-layer and amorphous *i*-layer.[5] This suggestion was confirmed by our simulation results,[7] using AMPS model developed at Penn State University.[8] Indeed, a "good" *μc*-Si:H *p*-layer with a large mean grain size (i.e., greater than 20 nm) and a large crystalline fraction should have a bandgap close to ~1.1 eV, the one of bulk crystalline silicon. However, if we could make a *μc*-Si:H *p*-layer with a wide bandgap, what will happen to the cells? And how can we make such a *p*-layer? One way to achieve a wide band gap *p*-layer is to use the QCE, i.e., to make *μc*-Si:H which comprise small Si nanocrystals embedded in an amorphous Si-H matrix. In this case the energy bangap of *μc*-Si:H should be enlarged by the QCE. In the following we prefer to use the term "nanocrystalline silicon", instead of "microcrystalline silicon" for such a kind of material. On the basis of the foregoing considerations it is appropriate in the present letter to identify the different effects of *nc*-Si:H and μc-Si:H *p*-layers on the performances of *a*-Si:H *n-i-p* cells.

Experimental

The *p*-layer samples were prepared using conventional rf (13.56 MHz) PECVD and a gas mixture of SiH$_4$, BF$_3$ and H$_2$ in an ultrahigh-vacuum, multi-chamber, load-locked deposition system. For growing *nc*-Si:H *p*-layers we used a high hydrogen dilution (H$_2$/SiH$_4$=166) and a high gas pressure of 2 Torr as well as a high power density of 1.0 W/cm^2 at a low substrate temperature of 70°C. To increase microcrystallinity in the μc-Si *p*-layers, the deposition parameters were changed to a higher hydrogen dilution (H$_2$/SiH$_4$=200), a low gas pressure of 0.6 Torr as well as a low power density of 35mW/cm^2 at 200°C. Samples for use in *a*-Si:H *n-i-p* cells have a structure of SS/Al/ZnO/*n-a*-Si:H/*i-a*-Si:H/*p*-Si:H/ITO, with a protocrystalline *i*-layer deposited using a gas mixture of Si$_2$H$_6$ and H$_2$ at a high hydrogen dilution (H$_2$/Si$_2$H$_6$=100) at 200°C. To enhance the

formation of nanocrystalline nucleation sites for the *p*-layer deposition, we inserted a seed layer between the *p*- and *i*-layer in the samples. For analyses of the optical and structural properties the *p*-layer samples were deposited on Corning 7059 glass using the identical conditions as used in the solar cells, but with different deposition times. The formation of silicon nanocrystals and their mean grain size in the samples were characterized by Raman scattering and TEM. In view of the fact that microcrystalline growth is sensitive to the substrate material and the accumulated thickness,[9] we also made a thin sub-seed and *i*-layer (15 nm) before the *p*-layer deposition on Corning 7059 glass, simulating the p/i interface structure of the cell samples, and took the Raman signals from both sides, the front surface and the back surface through the glass substrate.

Results and Discussions

The obtained Raman spectra for the *nc*-Si:H and μc-Si:H *p*-layer samples are given in Fig.1, which were recorded near backscattering geometry using an Ar$^+$ laser operating at a wavelength of 488 nm and a double monochrometer in the silicon TO mode region. Curve (a) of Fig.1 shows the Raman spectrum of the μc-Si *p*-layer sample (~50 nm thick). This curve has a sharp peak at 521 cm^{-1}, which is typical for bulk crystalline Si. Curve (b) and (c) of Fig.1 are the spectra of the *nc*-Si:H *p*-layer sample (~350 nm thick), taken from the front surface and the back surface through the glass substrate, respectively. As generally observed with *nc*-Si:H, two peaks appear in the spectra, a broad peak at 480 cm^{-1}, which is characteristic of amorphous Si and a sharp peak at 514 cm^{-1}, which is characteristic of Si nanocrystals. It is seen that Curve (b) is dominated by the sharp peak at 514 cm^{-1}, while Curve (c) comprises a broad peak at 480 cm^{-1} and a small shoulder at ~514cm^{-1}, demonstrating the reported dependence of crystallinity on the accumulated thickness.[9] The Gaussian deconvolution of the two Raman spectra data are listed in table 1, including the peak position (P$_k$), the peak area (A) of the TO modes and the volume crystalline fraction (C), which was determined using the ratio of peak area of crystalline to that of amorphous inclusions with a cross section ratio of 0.9.[10] As can be seen that the Raman spectrum taken from the backside shows a less volume crystalline fraction, although it has nearly the same Raman redshift of 7 cm^{-1} with respect to the TO phonon mode in bulk crystalline Si. From this Raman redshift, we deduced the mean nanocrystal size to be 2.1 nm or 2.5 nm, according to a bond polarizability model of J. Zi *et al.*,[11] or a modified phonon confinement model of Campbell and Fauchet.[12,13] These estimated sizes might be smaller than the actual sizes, due to an overestimate of the phonon confinement effect without considering the existence of tensile stress in the film.[14]

Table 1. Gaussion deconvolution of the Raman spectra of Curve (b) and Curve (c) in Fig.1, including the peak position (P$_k$) and the peak area (A) of the TO modes for crystalline (TO$_c$), amorphous (TO$_a$) and interfacial (TO$_i$) inclusions. The volume crystalline fraction (C) is also listed.

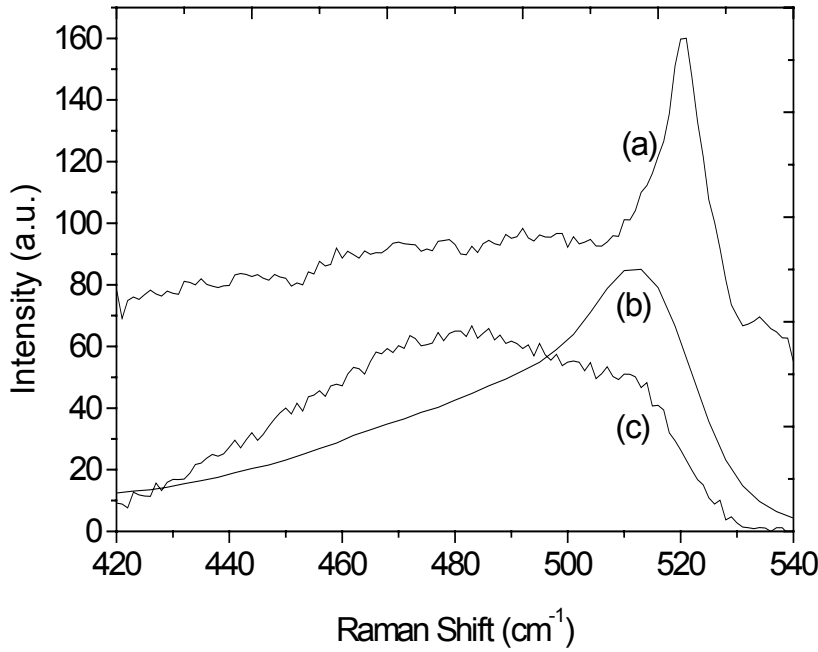| nc-Si p-layer	TO$_c$		TO$_i$		TO$_a$		C
	Pk(cm^{-1})	A(a.u.)	Pk(cm^{-1})	A(a.u.)	Pk(cm^{-1})	A(a.u.)	
Top surface	514.2	87653	500.1	51031	480.2	194436	0.44
Back surface	514.0	52662	500.6	70339	480.3	228673	0.37

Figure1. Raman spectra of the μc-Si:H *p*-layer (Curve a) and the *nc*-Si:H *p*-layer samples taken from the front surface (Curve b) and the back surface (Curve c) through the glass substrate.

In order to characterize the crystallization in a very thin *p*-layer, a JEOL 2010F STEM/TEM microscope was used. The films were lifted off from glass substrate by etching with a diluted HF solution and supported by a copper TEM grids. The thin *p*-layer sample has a hybrid, stacked structure, comprising a 15 nm thick *p*-layer on a 15 nm *i*-layer with a seed layer in between, which was deposited under identical conditions as those used in solar cells. Fig. 2(a) shows a high-angle annular dark-field (HAADF) image of the sample, where many separated bright dots were observed, which represent nanocrystalline particles. Most of the particles are ranging from 3 to 5 nm, larger than the estimated values from Raman study. Several large white dots in this figure are the clusters of 3 or 4 crystalline particles. In the insert a selected-area electron diffraction (SAED) is illustrated, indicating diffraction pattern with crystalline feature for the area probed. Fig. 2(b) shows a high-resolution electron microscopy (HREM) image, exhibiting the lattice image. The interference fringes separated by 0.31 nm correspond to the spacing of Si (111) planes of the nanocrystals. Fig. 2 (c) is a nano electron diffraction (NED) taken from one of the bright dots indicating the crystalline nature of the particle. These images clearly demonstrate that the *p*-layer deposited at a low substrate temperature and a high hydrogen dilution contains nanocrystalline Si particles of 3-5 nm in size. We estimated the effective energy bandgap of these Si nanocrystals should be enlarged to 2.3-1.9 eV, if it is treated as isolated spherical quantum dots saturated with hydrogen, based on the density-function approach of B. Delley and E.F. Steigmeier.[15] In fact the optical transmittance measurements performed on the same *nc*-Si:H *p*-layer sample used in the Raman scattering (Fig. 1) show that its Tauc optical bandgap is about 1.96 eV, confirming that the *nc*-Si:H *p*-layer indeed possesses a wide bandgap. However, one could not simply compare the Tauc bandgap value with the above theoretical estimate, because the former is an effective bandgap width of a diphasic material with an indirect gap, while the latter is for isolated Si quantum dots.

Effectiveness of a thin *nc*-Si:H *p*-layer for a solar cell can be most convincingly judged in a cell configuration. We prepared *n-i-p* *a*-Si:H solar cells at a similar condition but using a *nc*-Si:H or µc-Si:H *p*-layer. The resultant typical *I-V* curves are demonstrated in Fig.3. It is observed that using a *nc*-Si:H p-layer the cell performances (Curve a) could be enhanced, with a V_{oc} of 1.042 V, a *FF* of 0.734, a short circuit current of 11.6 mA/cm^2, and an efficiency of 8.87 %, while incorporating a µc-Si:H *p*-layer into the cell (Curve b), the V_{oc} decreased to 0.526 V.
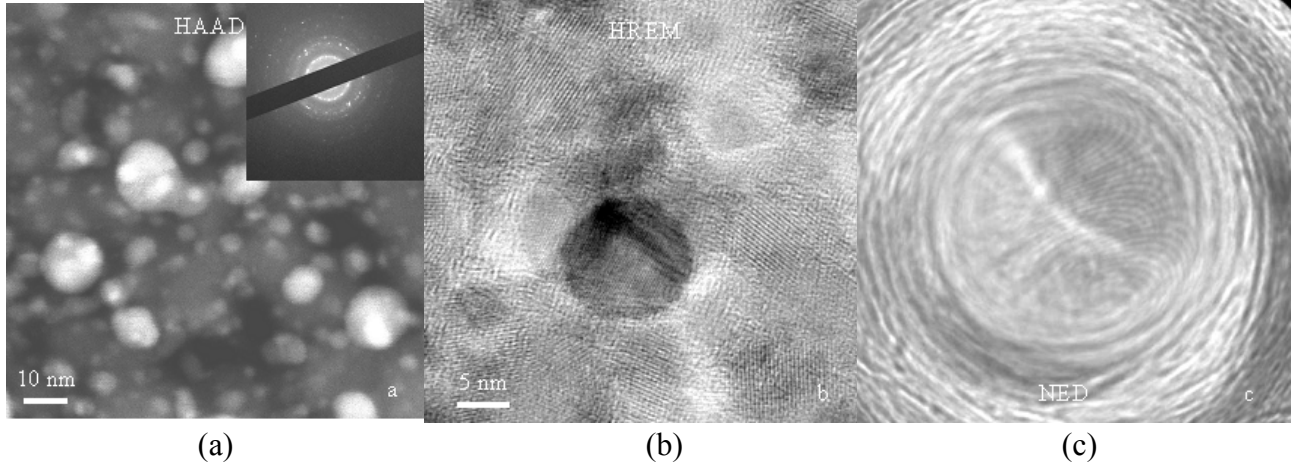

(a) (b) (c)

Figure 2. TEM micrographs of a thin *nc*-Si:H *p*-layer of 30 nm thick with a hybrid, stacked structure. (a) HAADF image, where bright dots represent nanocrystalline particles; in the insert is a SAED image, showing the diffraction pattern with crystalline features; (b) HREM image, exhibiting the lattice image; (c) NED image, indicating a formation of a crystal particle
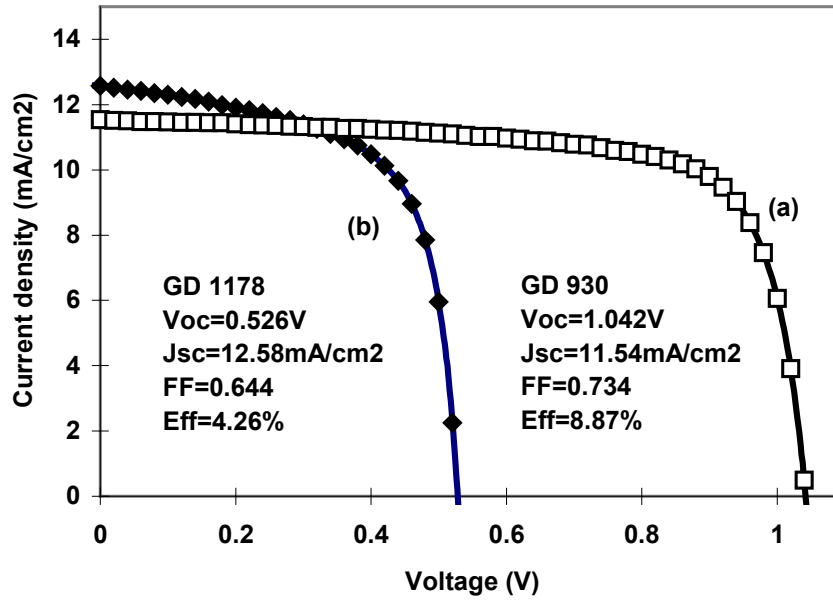

Figure 3. *I-V* characteristics of *n-i-p* *a*-Si:H solar cells on SS coated with Al/ZnO using the *nc*-Si:H *p*-layer (Curve a) or µc-Si:H *p*-layer (Curve b) as the window layer.

References

1. T. Tiedje, Appl. Phys. Lett. **40**, 627 (1982).
2. B.Yan, J. Yang, and S. Guha, Appl. Phys. Lett. **83**, 782 (2003).
3. S. Tsuge, Y. Hishikawa, S. Okamoto, M. Sasaki, S. Tsuda, S. Nakano, and Y. Kuwano, Mat. Rec. Soc. Symp. Proc. **258**, 869(1992).
4. S. Guha, J. Yang, P. Nath, and M. Hack, Appl. Phys. Lett. **49**, 218 (1986)
5. J. K. Rath, and R. E. I. Schropp, Solar Energy Materials and Solar Cells **53,** 189(1998).
6. R. J. Koval, Chi Chen, G. M. Ferreira, A. S. Ferlauto, J. M. Pearce, P. I. Rovira, C. R. Wronski, and R. W. Collins, Appl. Phys. Lett. **81**, 1258 (2002).
7. X. Liao, W. Wang and X. Deng, Proc. 29th IEEE-PVSC, 1234 (2002).
8. For AMPS, see http://www.psu.edu/dept/AMPS/.
9. Joohyun Koh, A. S. Ferlauto, P. I. Rovira, C. R. Wronski, and R. W. Collins, Appl. Phys. Lett. **75**, 2286 (1999)
10. G. Yue, J. D. Lorentzen, J. Lin, D. Han, and Q Wang, Appl. Phys. Lett. **75**, 492 (1999).
11. J. Zi, H. Buescher, C. Falter, W. Ludwig, K. Zhang and X. Xie, Appl. Phys. Lett. **69**, 200 (1996)
12. Ch. Ossadnika, S. Veprek, and I. Gregora, Thin Solid Films **337**, 148 (1999).
13. I. H. Campbell, P.M. Fauchet, Solid State Commun. **58**, 739 (1986).
14. V. Paillard, P. Puech, R. Sirvin, S. Hamma and P. Roca i Cabarrocas, J. Appl. Phys. **90**, 3276 (2001).
15. B. Delley and E.F. Steigmeier, Phys. Rev. **B 47**, 1397 (1997).